Through-Bond Exchange Coupling and Triplet Excitons in a Dinuclear Copper(II) Macrocyclic Complex

Jean Christophe Colin,[1a] Talal Mallah,[1b] Yves Journaux,*[,1a] Francesc Lloret,[1c] Miguel Julve,[1c] and Claudette Bois[1b]

Laboratoire de Chimie Inorganique, URA CNRS No. 420, Université de Paris-Sud, 91405 Orsay, France, Departament de Quimica Inorgànica, Facultat de Quïmica de la Universitat de València, Dr Moliner 50, 46100-Burjassot (València), Spain, and Laboratoire de Chimie des Métaux de Transition, URA CNRS No. 419, Université Pierre et Marie Curie, 75252 Paris, France

Received February 17, 1995[⊗]

The reaction of the bicyclic cryptand 1,4,7,10,13,16,21,24-octaazabicyclo[8.8.8]hexacosan-5,6,14,15,22,23-hexone (**1**) with copper(II) leads to the dinuclear complex {1,10-bis(2-aminoethyl)-1,4,7,10,13,16-hexaazacyclooctadecane-5,6,14,15-tetronato(4−)}dicopper(II) (**2**). **2** crystallizes in the triclinic system (space group $P\bar{1}$, No. 2), with cell parameters $a = 6.751(1)$ Å, $b = 10.153(1)$ Å, $c = 10.748(2)$ Å, $\alpha = 71.83(1)°$, $\beta = 89.79(1)°$, $\gamma = 73.56(1)°$, and $Z = 1$. The structure is made up of centrosymmetric neutral dinuclear copper(II) units stacking along the *a* axis. Each copper(II) ion assumed a distorted-octahedral environment. The basal positions are occupied by four nitrogen atoms, two from deprotonated amide groups and two from the tertiary and primary amines; the apical positions are occupied by one amido nitrogen atom from the same dimer and one amido oxygen atom from a neighboring unit within the stack. The analysis of variable-temperature magnetic susceptibility data reveals the occurrence of a significant intramolecular antiferromagnetic interaction ($J = -47$ cm^{-1}) in **2**. The analysis of the exchange pathways by extended Hückel calculations shows a strong contribution of the N−C−C−N σ bonds to the coupling between the two copper(II) ions. The triplet exciton type EPR spectrum of **2** allowed the evaluation of the interdimer interaction ($J' \approx 10^{-3}$ cm^{-1}), a possible description of **2** as a magnetic alternating chain being ruled out.

Introduction

Oxamido-based complexes with transition-metal ions have proved to be good molecular precursors to synthesize polynuclear complexes.[2,3] In our laboratory, we have developed the synthesis of a macrobicyclic ligand containing six oxamide and two amine functions. The reaction between tris(2-((ethyloxomoyl)oxy)ethyl)amine (trenest) and tris(2-aminoethyl)amine (tren) using high-dilution techniques provides the pure macrobicyclic ligand 1,4,7,10,13,16,21,24-octaazabicyclo[8.8.8]hexacosane-5,6,14,15,22,23-hexone (**1**) (Chart 1).

The acid−base and coordinating properties of **1** have been investigated by potentiometry,[4] which revealed the existence of a copper(II)-assisted hydrolytic reaction of **1** in basic medium leading to the dinuclear complex {1,10-bis(2-aminoethyl)-1,4,7,-10,13,16-hexaazacyclooctadecane-5,6,14,15-tetronato(4−)}dicopper(II) (**2**). **2** contains a new macrocyclic ligand derived from **1** by loss of an oxalato anion (Chart 2).

Chart 1

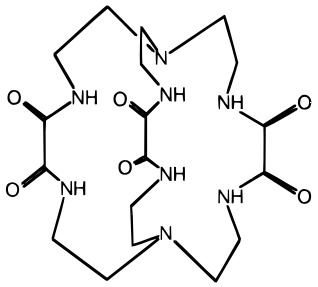

1

Chart 2

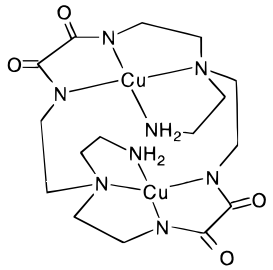

2

We report here the synthesis, the structural characterization, magnetic properties, and EPR spectra of **2**.

Experimental Section

Materials. Tris(2-aminoethyl)amine (tren) was purchased from Aldrich and distilled before use. Ethyl oxamate, diethyl oxalate, $Cu(CH_3COO)_2 \cdot H_2O$ were of reagent grade quality. They were purchased from commercial sources and used as received.

⊗ Abstract published in *Advance ACS Abstracts,* May 15, 1996.

(1) (a) Université de Paris-Sud. (b) Université Pierre et Marie Curie. (c) Universitat de València.

(2) (a) Ojima, H.; Nonoyama, K. *Coord. Chem. Rev.* **1988**, *92*, 85. (b) Journaux, Y.; Sletten, J.; Kahn, O. *Inorg. Chem.* **1985**, *24*, 4063. (c) Christodoulou, D.; Kanatzidis, M. G.; Coucouvanis, D. *Inorg. Chem.* **1990**, *29*, 191. (d) Nakatani, K.; Carriat, J. Y.; Journaux, Y.; Kahn, O.; Lloret, F.; Renard, J. P.; Pei, Y.; Sletten, J.; Verdaguer, M. *J. Am. Chem. Soc*. **1989**, *111*, 5739.

(3) (a) Lloret, F.; Julve, M.; Faus, J.; Journaux, Y.; Philoche-Levisalles, M.; Jeannin, Y. *Inorg. Chem.* **1989**, *28*, 3702. (b) Lloret, F.; Sletten, J.; Ruiz, R.; Julve, M.; Faus, J.; Verdaguer, M. *Inorg. Chem.* **1992**, *31*, 778. (c) Lloret, F.; Julve, M.; Faus, J.; Ruiz, R.; Castro, I.; Mollar, M.; Philoche-Levisalles, M. *Inorg. Chem.* **1992**, *31*, 784. (d) Lloret, F.; Julve, M.; Real, J. A.; Faus, J.; Ruiz, R.; Mollar, M.; Castro, I.; Bois, C. *Inorg. Chem.* **1992**, *31*, 2956. (e) Real, J. A.; Mollar, M.; Ruiz, R.; Faus, J.; Lloret, F.; Julve, M.; Philoche-Levisalles, M. *J. Chem. Soc., Dalton Trans*. **1993**, 1483.

(4) Colin, J. C.; Mallah, T; Journaux, Y.; Mollar, M.; Lloret, F.; Julve, M.; Boubekeur, K. *Inorg. Chim. Acta*. **1996**, *246*, 1.

S0020-1669(95)00186-8 CCC: $12.00

Synthesis of Tris(2-(ethyl(oxy(oxamoyl)))ethyl)amine (trenest). A 7.3 g (0.05 mol) amount of tren dissolved in 200 mL of THF was added dropwise to 150 mL (large excess) of pure diethyl oxalate with vigorous stirring, over 3 h. The resulting liquid was reduced by removing the THF on a rotary evaporator. The yellow liquid obtained was treated with 750 mL of diethyl ether. Impure crystals of trenest appeared after 24 h. They were filtered, washed with ether, and then eluted through a silica column using a 95/5 (v/v) mixture of ethyl acetate and ethanol. Although several products separate, only the first one was collected, and 90% of the eluent was then evaporated. The concentrated solution was left to evaporate slowly overnight. Large (1 cm × 1 cm) transparent crystals grew during the night; yield 70%. ^{1}H NMR ($CDCl_3$ + TMS): δ 7.61 (broad t, 3H), 4.34 (q, 6H), 3.40 (t, 6H), 2.71 (t, 6H), 1.38 (t, 9H). Anal. Calcd for $C_{18}H_{30}N_4O_9$: C, 48.51; H, 6.67; N, 12.68; O, 32.44. Found: C, 48.53; H, 6.74; N, 12.56; O, 32.36.

Synthesis of 1,4,7,10,13,16,21,24-Octaazabicyclo[8.8.8]hexacosane-5,6,14,15,22,23-hexone (1). 1 was obtained by using a high-dilution technique: ethanolic equimolar solutions (0.1−0.2 mol dm^{-3}) of tren and trenest were added simultaneously dropwise into a 2 dm^3 round-bottom flask containing 1.2 dm^3 of vigorously stirred EtOH. The round-bottom flask was modified for more efficient stirring.[5] The level of the burets containing the two starting materials must never differ by more than 0.4 mL in order to avoid the formation of polymers. When 200 mL of the starting solutions was added, the resulting mixture was filtered and evaporated to 100−150 mL by using a rotary evaporator. The remaining solution was left overnight, and the white precipitate that formed was filtered and dried under vacuum; yield 77% and purity around 95%. This solid was purified by extraction with ethanol in a Soxhlet apparatus over 2 weeks. Pure compound **1** (H_6L) was obtained by evaporation of the solvent. ^{1}H NMR H_6L (pH >10, D_2O + DSS): δ 3.36 (broad t, 12H), 2.62 (broad t, 12H). Mass spectroscopy (positive ion $(M + H^+)^+$): *m/e* 455. Anal. Calcd for $C_{18}H_{30}N_8O_6$ (**1**): C, 47.58; H, 6.61; N, 24.67; O, 21.14. Found: C, 47.31; H, 6.63; N, 24.61; O, 21.44.

Synthesis of {1,10-Bis(2-aminoethyl)-1,4,7,10,13,16-hexaazacyclooctadecane-5,6,14,15-tetronato(4−)}dicopper(II) (2). A 1 mmol (454.5 mg) amount of **1** and 2 mmol (399.3 mg) of copper(II) acetate hydrate were added to 50 mL of water, giving a green suspension. An aqueous solution of 1 mol dm^{-3} sodium hydroxide was added slowly until a blue solution was obtained (pH *ca*. 14). This solution turned violet, and single crystals of **2** together with a few single crystals of **1** separated within a few days. The crystals of **1** were separated by the flotation method in chloroform, and those of **2** were filtered and dried under vacuum. The structure of **2** was determined by using these crystals. Anal. Calcd for $C_{16}H_{44}Cu_2N_8O_{12}$: C, 28.78; H, 6.64; N, 16.78; Cu, 19.04. Found: C, 28.70; H, 6.55; N, 16.50; Cu, 18.90.

Physical Techniques. Magnetic measurements of **2** were carried out on polycrystalline samples with a Faraday-type magnetometer equipped with a helium continuous-flow cryostat working in the 4.2−300 K temperature range. The independence of the susceptibility versus the applied field was checked at room temperature for all compounds. Mercury tetrakis(thiocyanato)cobaltate(II) was used as a susceptibility standard. Diamagnetic corrections were estimated as -336×10^{-6} cm^3 mol^{-1}. EPR spectra of **2** were recorded on powder samples at X-band frequency with a Brüker ER 200D spectrometer equipped with a cryostat working in the 4.2−300 K temperature range, an NMR probe, and a Hewlett-Packard 5350B microwave frequency counter.

NMR spectra were recorded on a Brüker AC 250 NMR spectrometer operating at 250 MHz for ^{1}H. ^{1}H NMR spectra were performed in $CDCl_3$ or in D_2O, the internal standard being TMS for the former and DSS or dioxane for the latter. Mass spectra were recorded on a NERMAG R-10-10 using DCI with NH_3.

Crystallographic Data Collection and Structure Determination of 2. All measurements were carried out on an Enraf-Nonius CAD4 diffractometer by using graphite-monochromated Mo Kα (λ = 0.710 73 Å) radiation and $\omega/2\theta$ scans. A prismatic crystal of **2** with approximate dimensions 0.6 × 0.5 × 0.35 mm was mounted on the diffractometer and used for data collection. Cell dimensions were obtained from least-squares refinement of 25 reflections in the 2θ range 14−15°. The crystal data are summarized in Table 1. The intensities of three standard reflections for **2** decrease by 10% over the period of the experiment, and a correction was applied. Intensity data were collected in the θ range 1−25°, the scan width being 0.8 + 0.34 tan θ. Lorentz and polarization effects were accounted for, but not absorption. Of the 1856 measured independent reflections, 1512 were unique with $I > 3\sigma(I)$ and were used in the structure determination. On the basis of the centric distribution of E values, $P\bar{1}$ space group was assumed for **2** and later confirmed by the successful refinement of the structure. The structure of **2** was solved by Patterson methods, followed by successive Fourier syntheses. Refinement was performed with the full-matrix least-squares method in one block (173 parameters) with anisotropic thermal parameters for all non-hydrogen atoms. Hydrogen atoms were located in difference-Fourier maps and were given an isotropic thermal parameter. The quantity minimized was $\sum w(\Delta F)^2$, with unit weights. No secondary extinction correction was considered. Neutral-atom scattering factors[6] and anomalous dispersion terms[7,8] were taken from the usual sources. The refinements converged at $R = 0.042$ and $R_w = 0.048$. The final difference Fourier map shows residual maxima and minima of 0.93 and −0.66 e Å^{-3}. All calculations for **2** were carried

Table 1. Crystallographic Data for **2**

compd	2
formula	$C_{16}H_{44}Cu_2N_8O_{12}$
fw	667.7
space group	$P\bar{1}$
a, Å	6.751(1)
b, Å	10.153(1)
c, Å	10.748(2)
α, deg	71.83(1)
β, deg	89.79(1)
γ, deg	73.56(1)
V, Å^3	668.4(7)
Z	1
temp, °C	18
λ(Mo Kα), Å	0.710 73
ρ_{calcd}, g cm^{-3}	1.66
μ(Mo Kα), cm^{-1}	16.6
$R = \sum\|F\|/\sum\|F_o\|$	0.042
$R_w = [\sum w(\Delta F)^2/\sum wF_o^2]^{1/2}$	0.048

Table 2. Atomic Coordinates and Thermal Parameters[a,b] for Non-Hydrogen Atoms of **2**

atom	x/a	y/b	z/c	U(eq), Å^2
Cu(1)	0.1386(1)	0.03509(8)	−0.10466(7)	0.0243
N(1)	0.0723(7)	0.0239(5)	−0.2874(4)	0.0210
N(2)	0.3136(7)	−0.1588(5)	−0.0748(5)	0.0259
N(3)	0.2330(7)	−0.0037(5)	0.0824(4)	0.0179
N(4)	0.0340(8)	0.2505(5)	−0.1857(5)	0.0312
C(1)	0.2588(9)	−0.0847(7)	−0.3058(6)	0.0305
C(2)	0.3233(9)	−0.2164(7)	−0.1829(6)	0.0284
C(3)	0.4326(9)	−0.2187(6)	0.0341(6)	0.0266
C(4)	0.3978(8)	−0.1220(6)	0.1226(6)	0.0232
C(5)	0.1918(9)	0.0889(6)	0.1628(6)	0.0246
C(6)	0.1214(9)	0.0199(6)	0.2968(6)	0.0232
C(7)	0.0460(9)	0.1726(7)	−0.3783(6)	0.0316
C(8)	−0.068(1)	0.2850(6)	−0.3178(6)	0.0334
O(1)	0.5717(7)	−0.3395(5)	0.0727(4)	0.0424
O(2)	0.5199(6)	−0.1583(5)	0.2211(4)	0.0355
O(3)	0.1126(8)	0.3570(6)	−0.6894(5)	0.0560
O(4)	0.453(1)	0.3253(7)	−0.5204(6)	0.0742
O(5)	0.3008(8)	0.5054(6)	−0.3412(5)	0.0629
O(6)	0.192(1)	0.5088(6)	0.0603(6)	0.0680

[a] Estimated standard deviations in the last significant digits are given in parentheses. [b] Anisotropically refined atoms are given in the form of the isotropic equivalent displacement parameter, defined as one-third of the trace of the orthogonalized $\mathbf{U}_{ij}$ tensor.

(5) Dietrich, B.; Lehn, J. M.; Sauvage, J. P.; Blanzat, J. *Tetrahedron* **1973**, *29*, 1629.

(6) Cromer, D. T.; Waber, J. T. In *International Tables for X-ray Crystallography*; Kynoch Press: Birmingham, England, 1974; Vol. IV, Table 2.2A.

(7) Ibers, J. A.; Hamilton, W. C. *Acta Crystallogr.* **1974**, *17*, 781.

(8) In ref 6, Table 2.3.1.

Table 3. Selected Bond Lengths (Å) and Angles (deg) Involving Non-Hydrogen Atoms of **2**[a,b]

Cu(1)−Cu(1)′	2.966(1)	Cu(1)−N(1)	2.061(4)
Cu(1)−N(2)	1.915(5)	Cu(1)−N(3)	1.994(4)
Cu(1)−N(4)	1.995(5)	N(1)−C(1)	1.479(7)
N(1)−C(6)	1.508(7)	N(1)−C(7)	1.481(7)
N(2)−C(2)	1.449(7)	N(2)−C(3)	1.292(7)
N(3)−C(4)	1.338(7)	N(3)−C(5)	1.437(7)
N(4)−C(8)	1.474(8)	C(1)−C(2)	1.515(9)
C(3)−C(4)	1.541(8)	C(3)−O(1)	1.261(7)
C(4)−O(2)	1.236(7)	C(5)−C(6)	1.532(8)
C(7)−C(8)	1.509(9)		
N(1)−Cu(1)−Cu(1)′	119.2(1)	N(2)−Cu(1)−Cu(1)′	97.3(1)
N(2)−Cu(1)−N(1)	83.3(2)	N(3)−Cu(1)−Cu(1)′	60.0(1)
N(3)−Cu(1)−N(1)	166.6(2)	N(3)−Cu(1)−N(2)	83.6(2)
N(4)−Cu(1)−Cu(1)′	104.5(1)	N(4)−Cu(1)−N(1)	86.9(2)
N(4)−Cu(1)−N(2)	158.1(2)	N(4)−Cu(1)−N(3)	106.3(2)
C(1)−N(1)−Cu(1)	103.7(3)	C(6)−N(1)−Cu(1)	113.1(3)
C(6)−N(1)−C(1)	111.7(4)	C(7)−N(1)−Cu(1)	104.3(3)
C(7)−N(1)−C(1)	113.2(4)	C(7)−N(1)−C(6)	110.5(4)
C(2)−N(2)−Cu(1)	117.3(4)	C(3)−N(2)−Cu(1)	116.3(4)
C(3)−N(2)−C(2)	125.7(5)	C(4)−N(3)−Cu(1)	110.0(4)
C(5)−N(3)−Cu(1)	130.9(4)	C(5)−N(3)−C(4)	116.8(5)
C(8)−N(4)−Cu(1)	108.6(4)	C(2)−C(1)−N(1)	110.5(5)
C(1)−C(2)−N(2)	105.3(5)	C(4)−C(3)−N(2)	112.7(5)
O(1)−C(3)−N(2)	129.0(6)	O(1)−C(3)−C(4)	118.2(5)
C(3)−C(4)−N(3)	114.7(5)	O(2)−C(4)−N(3)	126.4(5)
O(2)−C(4)−C(3)	119.0(5)	C(6)−C(5)−N(3)	113.5(4)
C(5)−C(6)−N(1)	113.5(4)	C(8)−C(7)−N(1)	111.0(5)
C(7)−C(8)−N(4)	109.1(5)		

[a] Estimated standard deviations in the last significant digits are given in parentheses. [b] The symmetry code denoted by a prime is $-x, -y, -z$.

out on a VAX725 station with the computer program CRYSTALS.[9] The molecular plots were drawn using the ORTEP and Molview programs.[10] Atomic parameters for non-hydrogen atoms are given in Table 2; bond lengths and angles for non-hydrogen atoms are listed in Table 3. Hydrogen-atom coordinates (Table SI), anisotropic thermal parameters for non-hydrogen atoms (Tables SII), least-squares planes (Tables SIII), and hydrogen bonds (Table SIV) are given as Supporting Information.

Results

Description of the Structures of 2. The structure of **2** is made up of centrosymmetric neutral dinuclear copper(II) complexes which crystallize with eight water molecules. A perspective view of the dinuclear complex is shown in Figure 1.

The dinuclear units are stacked along the *a* axis, forming a pseudo-chain as illustrated in Figure 2. Each stack of dinuclear units is isolated from its neighbors by water molecules of crystallization. The organic part of the molecule is formed by a monocycle containing two oxamido groups and two tertiary amine functions whose third substituents are 2-aminoethyl pendant groups, giving an octadentate ligand. This new ligand comes from the copper(II)-assisted hydrolysis of **1** by loss of one oxamide group[4]. The copper(II) ion has a 4 + 1 + 1 environment. The vertices of the basal plane are occupied by four nitrogen atoms: two amido N(2) and N(3) (1.915(5) and 1.994(4) Å for Cu(1)−N(2) and Cu(1)−N(3), respectively), one tertiary amine N(1) (2.061(4) Å for Cu(1)−N(1)), and one primary amine N(4) (1.995(5) Å for Cu(1)−(N4)). The two apical positions are occupied by one amido nitrogen atom N(3)′ ($-x, -y, -z$) (2.618(5) Å for Cu(1)−N(3)′) belonging to the same dinuclear unit and the oxygen atom O(2)″ ($1 - x, -y, -z$) (3.013(4) Å for Cu(1)−O(2)″) belonging to the neighboring molecule within the stack. Each copper(II) is displaced out of the mean equatorial plane toward the axial nitrogen atom N(3)′ by 0.162 Å. The intramolecular metal−metal separation (Cu(1)···Cu(1)′) is 2.966(1) Å, whereas the shortest intermolecular one (Cu(1)···Cu(1)″, $1 - x, -y, -z$) is 5.147(1) Å.

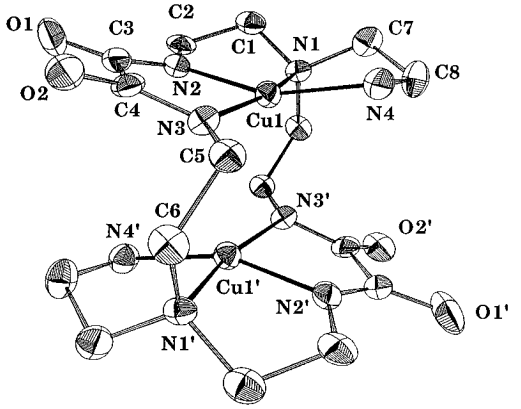

Figure 1. ORTEP view of **2** showing the atom-numbering scheme. Hydrogen atoms and water molecules are omitted for simplicity. Thermal ellipsoids are drawn at the 30% probability level.

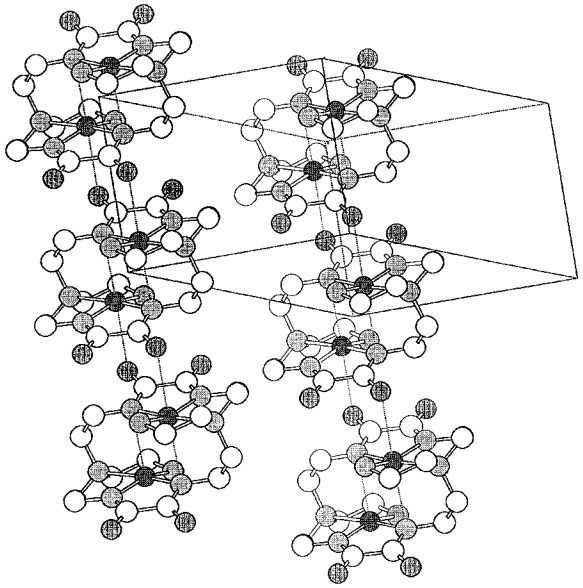

Figure 2. Drawing of **2** showing crystal packing. The *a* axis is vertical, whereas the *b* axis runs horizontally.

Magnetic Properties and EPR Spectroscopy of 2. The magnetic behavior of **2** is depicted in Figure 3 in the form of an χ_M versus T plot, χ_M being the magnetic susceptibility per two copper(II) ions. The value of χ_M is equal to 2.80×10^{-3} $cm^3\ mol^{-1}\ K^{-1}$ at room temperature, which is the expected value for two uncoupled copper(II) ions. When the temperature is lowered, the susceptibility increases, reaches a maximum at 43 K, and then decreases, indicating the occurrence of an antiferromagnetic exchange interaction between the two Cu(II) ions. Below 12 K, χ_M increases again due to the presence of paramagnetic impurities. The experimental data were fitted using the Bleaney−Bowers expression for a copper(II) dimer modified to take into account the paramagnetic impurities (eq 1), where N, g, β, k, and T have their usual meanings, J is the

$$\chi_M = \frac{2Ng^2\beta^2}{kT}\frac{1}{3 + \exp[-J/kT]}[1 - \rho] + \rho\frac{Ng^2\beta^2}{2kT} \quad (1)$$

(9) Carruthers, J. R.; Watkin, D. W. J. CRYSTALS, an advanced crystallographic computer program; University of Oxford, Chemical Crystallographic Laboratory: Oxford, England, 1985.

(10) Johnson, C. K. ORTEP; Report ORNL-3794; Oak Ridge National Laboratory: Oak Ridge TN, 1971. Cense, J. M. Molview, ENSCP, 11 rue P. et M. Curie, 75231 Paris Cedex 5, France.

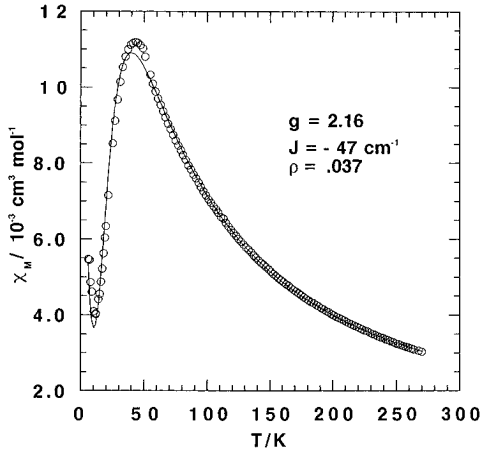

Figure 3. Temperature dependence for the molar magnetic susceptibility for **2**. Open circles and the continuous line correspond to the experimental data and the best theoretical fit, respectively.

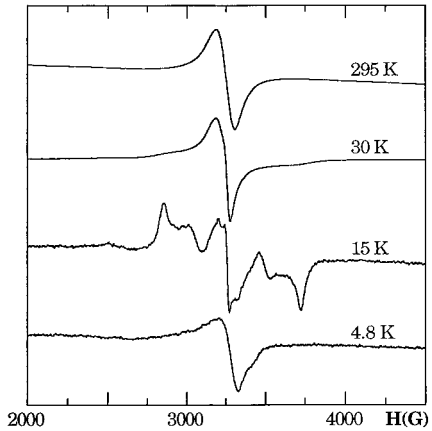

Figure 4. Temperature dependence of the X-band EPR spectra of polycrystalline samples of **2**.

singlet−triplet energy gap, and ρ is the amount of paramagnetic impurities (per two copper(II) ions). Values of J, g, and ρ of -47 cm^{-1}, 2.16, and 3.7% were obtained by least-squares fitting procedures with the agreement factor $R = 6 \times 10^{-5}$ (R is defined as $\sum[(\chi_M)_{obsd} - (\chi_M)_{calcd}]^2/\sum[(\chi_M)_{obsd}]^2$). In a second approach, the possible interaction between the copper(II) dimers through the weakly coordinated oxygen atoms of the neighboring molecules within the stack was taken into account and the magnetic data were fitted with the alternating chain model using the empirical expression proposed by Hatfield.[11] Values of J, α (exchange alternating parameter), g, and R of -48 cm^{-1}, 0.122, 2.23, and 3.9×10^{-4}, respectively, were found with this model. A comparison between both models reveals that the intramolecular exchange parameter J does not change significantly. Although the value of αJ (-5.9 cm^{-1}) seems too large for the interdimer interaction, the magnetic susceptibility data do not allow the exclusion of the description of the compound as an alternating chain. The complementarity between EPR and magnetic susceptibility measurements allows a conclusion to be drawn.

The EPR spectra of **2** at different temperatures are depicted in Figure 4. At liquid-helium temperature, the spectrum is consistent with a monomeric copper(II) impurity. Transitions associated with the excited triplet state appears when the sample is warmed. In the 9−20 K temperature range, the spectrum is typical of a triplet state with a half-field transition at 1590 G and the allowed transitions in the 2450−3750 G field range

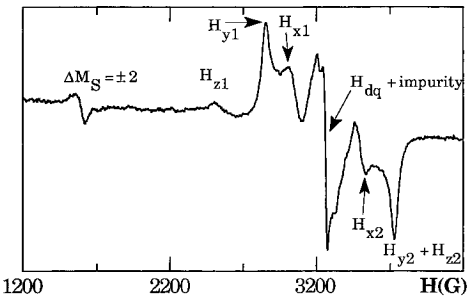

Figure 5. X-band EPR spectrum of **2** at 15 K.

(Figure 5). The main part of the spectrum exhibits six peaks, the central line being the superposition of the monomeric impurity and the double quantum transition. At 10 K, the experimental D and E values ($D = 0.065$ cm^{-1}, $E = 0.006$ cm^{-1}) are very different from those calculated for the point dipole approximation[12] ($D_{dip} = 0.212$ cm^{-1}, $E_{dip} = 0.0002$ cm^{-1}), strongly suggesting an anisotropic exchange contribution.[13] Above 20 K, the EPR lines broaden and the fine-structure splitting decreases. Finally, around 35 K the lines collapse into a singlet. At room temperature, the spectrum is nearly isotropic and is centered at $g = 2.065$. The half-field transition has completely disappeared. This change from a multiplet to a single line when the temperature is increased is characteristic of triplet excitons.[14] At low temperature, only a few dinuclear complexes in the excited triplet state exist and a triplet type spectrum is observed. When the temperature is raised, on one hand the number of molecules in the triplet state increases due to the Boltzmann factor, whereas on the other hand, the triplet excitation can move from one site to its neighbors owing to the weak interaction along the stack of the dinuclear complexes. Finally, above 20 K the excitons begin to collide. The frequency of collision follows a temperature dependence given by eq 2.

$$\nu = \nu_0 \exp[-\Delta E/kT] \tag{2}$$

The exchange interaction between the excitons produces an averaging of the fine structure. For a single crystal, the decrease of the splitting between the two allowed transitions is related to the collision frequency by eq 3

$$d_0^2 - d^2 = 8\nu^2 \tag{3}$$

where d_0 and d are the line separations in the absence and presence of exchange interaction, respectively. When the lines collapse, an order of magnitude for the interaction between the dinuclear complexes[15] can be obtained through eq 4

$$\alpha J \approx h(\nu/\sqrt{\Gamma_0}) \tag{4}$$

with

$$\Gamma_0 = \frac{2 \exp[-J/kT]}{1 + 3 \exp[-J/kT]} \tag{5}$$

In order to obtain the best values of ν, ΔE and αJ, a two-steps

(11) Hatfield, W. E. *J. Appl. Phys.* **1981**, *52*, 1985.

(12) Bencini, A.; Gatteschi, D. *EPR of Exchange Coupled Systems*; Springer-Verlag: Berlin, 1990; p 22.

(13) (a) Banci, L.; Bencini, A.; Gatteschi, D. *J. Am. Chem. Soc.* **1983**, *105*, 761. (b) Boillot, M. L.; Journaux, Y.; Bencini, A.; Gatteschi, D.; Kahn, O. *Inorg. Chem.* **1985**, *24*, 263. (c) Reference 12, p 27.

(14) (a) Chesnut, D. B.; Phillips, W. D. *J. Chem. Phys.* **1961**, *35*, 1002. (b) Reference 12, p 253. (c) Hoffmann, S. K.; Corvan, P. J.; Singh, P.; Sethulekshmi, C. N.; Metzger, R. M.; Hatfield, W. E. *J. Am. Chem. Soc.* **1983**, *105*, 4608.

(15) Blanc, J. P.; Dugay, M.; Robert, H.; Thibaud, C. *Phys. Status. Solidi* **1981**, *105*, 659.

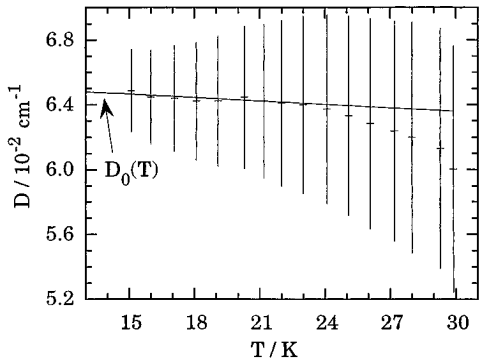

Figure 6. Thermal dependence of D for **2**.

Table 4. Structural Data, Isotropic Exchange Parameters, and SOMO Compositions for **2** and Related Centrosymmetrical Dinuclear Copper(II) Complexes[a]

	Cu(salen)[18b,28]	Cu(dmg)Cl$_2$[29]	Cu(L)$_2$Cl$_2$[30]	**2**
bridge, X	phenolate, *O*	chloride, Cl	chloride, Cl	oxamidate, N
d_1	2.026	2.238	2.210	1.995
d_2	2.412	2.689	3.370	2.618
$d_{Cu\cdots Cu}$/Å	3.181	3.438	4.368	2.966
θ (deg)	91.16	88.00	101.0	78.76
θ/d_2	37.8	32.7	30.0	30.1
J (cm^{-1})	18.5	6.3	-7.4	−48.0
Δ (meV)	30.6	45.0	22.9	177.9
Cu, $d_{x^2-y^2}$[b]	712	714	718	673
Cu, d_{z^2}[b]	18	9	45	15
X, p_x[b]	274	267	303	365
X, p_z[b]	41	12	13	47

[a] Abbreviations used: salen = *N,N′*-disalicylideneethylenediamine; dmg = dimethylglyoxime; L = 2-methylpyridine. [b] AO coefficients ($\times 10^3$).

procedure is used. First, the best D and E values at each temperature are obtained by fitting the powder spectrum using Wasserman's equations.[16] The temperature dependence of D is shown in Figure 6. Second, the line separation d for the transitions when $H \| z$ is calculated by using the best D and E parameters determined above.[17] The values of the activation energy ΔE and the collision frequency are evaluated to be 35 $\pm$ 20 cm^{-1} and $\nu_0 = 0.2 \pm 0.15$ GHz, respectively. αJ is then on the order of 10^{-3} cm^{-1}. This very small value for the interdimer interaction rules out the alternating-chain model. Nevertheless, despite the huge ratio between the values of the intra- and interdimer interactions, the weakest interaction is clearly visible on the EPR spectra.

Discussion

As is illustated in Table 4, for structurally related oxygen- or halogen-bridged copper(II) dinuclear complexes, the observed J values are very weak (a few cm^{-1}) and can be either positive or negative, depending on the bridging Cu−X−Cu angle (θ) and on the out-of-plane bond distance (d_2).[18] Hatfield has proposed the examination of the singlet−triplet splitting for parallel planar copper(II) dimers in terms of the ratio θ/d_2 (see Chart 3). In **2**, this parameter is equal to 30.1 and a weak coupling ($J \approx -7$ cm^{-1}) is expected (see Table 4); the observed

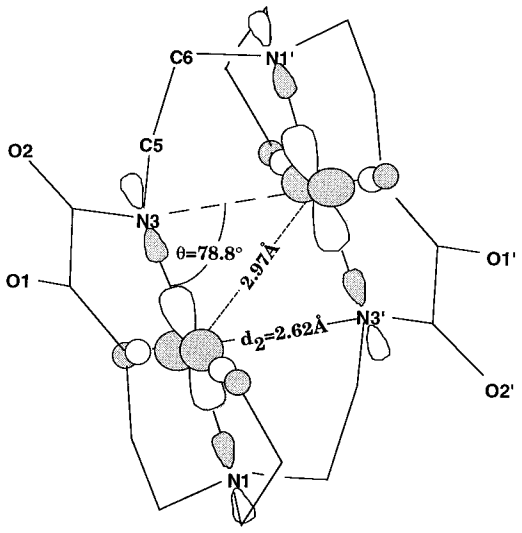

Figure 7. Relative orientation of the magnetic orbitals in **2**.

Chart 3

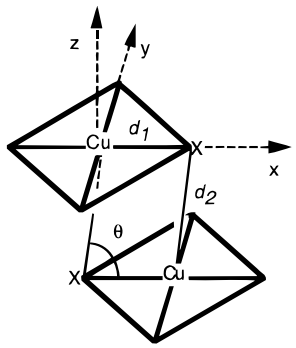

J value (−47 cm^{-1}) is unexpectedly large. Three superexchange pathways may occur in **2**: (i) direct interaction between copper(II) ions via a δ overlap of their $d_{x^2-y^2}$ orbitals, (ii) exchange coupling through the bridging amide nitrogens N3 (Figure 7), and (iii) superexchange through the N3−C5−C6−N1′ linkages which join the two parts of the complex (Figure 7). Extended Hückel calculations with FMO analysis by using the CACAO program[19] have been carried out in order to analyze the contribution of each exchange pathway to the overall superexchange interaction. According to current theoretical models, the square of the energy gap (Δ) between the symmetric (S) and antisymmetric (AS) MO's containing the two single electrons in the triplet state is proportional to the antiferromagnetic contribution.[20,21]

$$J_{AF} = \frac{\Delta^2}{j_0 - j} \tag{6}$$

where j_0 and j are the one-center and two-center Coulomb repulsion integrals, respectively. This gap is found to be equal to 178 meV in **2**, which is at least four times larger than those of the other dinuclear complexes (see Table 4).[22] All these compounds are widely different, but the difference between the

(16) Wasserman, E.; Snyder, L. C.; Yager, W. A. *J. Chem. Phys.* **1964**, *41*, 1763.
(17) The thermally corrected splitting d_0 is obtained by using Chesnut's procedure in order to take into account the dilation effect: Chesnut, D. B.; Meinholtz, D. C. *J. Chem. Phys.* **1984**, *80*, 3540.
(18) (a)Hatfield, W. E. In *Magneto-Stuctural Correlations in Exchange Coupled Systems*, Nato ASI Series C 140; Willett, R. D., Gatteschi, D., Kahn, O., Eds.; D. Reidel: Dordrecht, The Netherlands,1985; p 555. (b) Simpson, G. D.; Carlisle, G. O.; Hatfield, W. E. *J. Inorg. Nucl. Chem.* **1974**, *36*, 2257.
(19) Meallli,C.; Proserpio, D. M. *J. Chem. Educ.* **1990**, *67*, 399.
(20) Hay, P. J.; Thibeault, J. C.; Hoffmann, R. *J. Am. Chem. Soc.* **1975**, *97*, 4884.
(21) Kahn, O. In *Molecular Magnetism*; VCH: Weinheim, Germany, 1993; p 145.
(22) Standard H_{ii} parameters were used, giving d orbital energies lower than that of the ligand ones in **2**, but this does not, in any event, affect the analysis of exchange mechanisms in **2**. Putting the d orbital energies higher than those of the ligand ones will only affect slightly the Δ value and the MO composition of **2**.

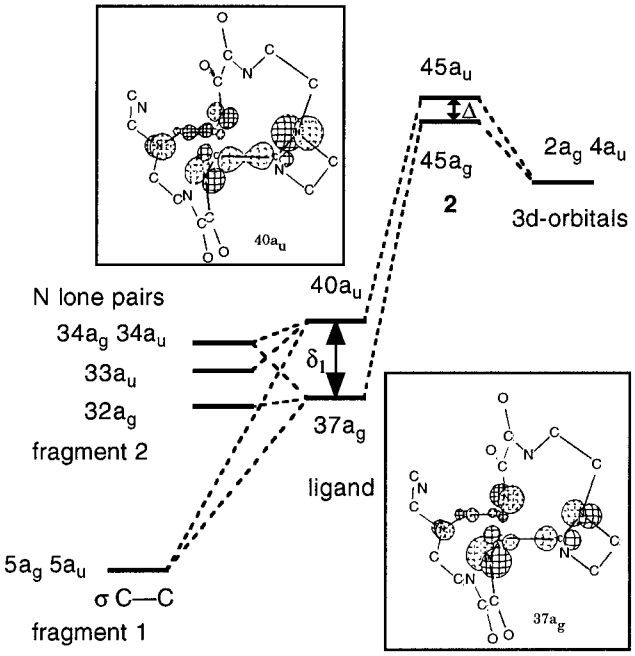

Figure 8. MO energy diagram illustrating the through-σ-bond mechanism in **2**. The atoms constituting of fragments 1 and 2 are C(5), C(6), H(9)−H(12), C(5)′, C(6)′, H(9)′−H(12)′ and C(1)−C(4), O(1), O(2), N(1)−N(4), H(1)−H(8), C(1)′−C(4)′, O(1)′, O(2)′, N(1)′-N(4)′, and H(1)′−H(8)′, respectively. Ligand is the abbreviation for 1,10-bis(2-aminoethyl)-1,4,7,10,13,16-hexaazacyclooctadecane-5,6,14,15-tetronato-(4−). For clarity, only the contributions of the bridging atoms to the 37a$_g$ and 40a$_u$ orbitals are represented.

calculated Δ value for **2** and for the other ones is significant within the framework of semi empirical extended Hückel calculations. The SOMO's in **2** can be mainly described as resulting from the interaction of the fragment orbitals (FMO's) of the fully deprotonated ligand (37a$_g$ and 40a$_u$) with the symmetric (S) and antisymmetric (AS) combination of $d_{x^2-y^2}$ metallic orbitals (2a$_g$ and 4a$_u$) (Figure 8).

The first exchange pathway, due to direct metal-metal interaction, may be easily ruled out. The intramolecular metal-metal distance (2.966 Å) and the relative orientation of the metallic orbitals as depicted in Figure 7 (weak overlap) lead to nearly degenerate FMO's 2a$_g$ and 4a$_u$, the energy separation being only 10 meV.

The exchange coupling through the bridging amide nitrogens N(3) (which is the second possible exchange pathway) can be analyzed by considering the structure parameters: each copper(II) ion is surrounded by a distorted square pyramid where the metal ion lies 0.162 Å above the basal plane toward the axial amide nitrogen N(3)′; the magnetic orbital[23] is then mainly of $d_{x^2-y^2}$ type in the equatorial plane with a small d_{z^2} axial component. On the bridging nitrogen N(3), the interaction between the equatorial $d_{x^2-y^2}$ spin density of one copper and the axial d_{z^2} spin density of the other leads to an antiferromagnetic coupling.[24] This interaction is, in general, very weak due to the small d_{z^2} axial component in the magnetic orbitals (Table 4), but in our specific case three factors may contribute to reinforce this pathway in **2**: (i) the value of the Cu(1)−N(3)′−Cu(1)′ angle (78.8(1)°), which is far from 90°, contributing to a better overlap of the magnetic orbitals, (ii) the better match in energy between the N(3) (or N(3)′) lone pairs and the metal

Chart 4

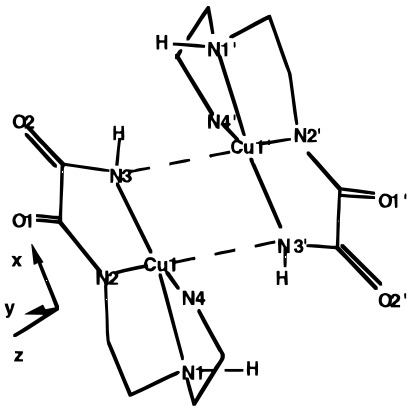

orbitals, this strongly basic amido nitrogen atom having its lone pair at higher energy (thus closer to metal orbitals) than *o*-phenolato or chlorine bridging atoms, (iii) the more diffuse character of the bridging amido nitrogen orbitals. These last two points lead to a large spin delocalization of the $d_{x^2-y^2}$ magnetic orbital onto the oxamidato N(3) atom and to a rather short Cu−N(3) distance (1.995 Å); this is illustrated by the contribution of the N(3) p_x orbital to the magnetic orbital being at least 20% greater in **2** than those of the related complexes (see Table 4).

This larger spin delocalization of the $d_{x^2-y^2}$ orbital onto the N(3) atom enhances the overlap between the two magnetic orbitals. To evaluate the contribution of this pathway to the total gap value (178 meV), we have calculated the gap value in a dinuclear Cu(II) model complex where the alkyl bridges were removed as shown in Chart 4. We found a Δ value equal to 36 meV. This value represents only 20% of the total gap, and consequently the second pathway is certainly not the predominant one. It is worthy of note that 36 meV is close to the calculated values for the related complexes, and this strongly suggests that another exchange mechanism is operative in **2** (Table 4). Nevertheless, we have tested the influence of electronegativity of the bridging atoms N(3) by changing the H_{ii} and ζ (Slater exponent) values of the oxamidato nitrogen atoms by those of oxygen atoms. As expected, the gap decreases to 22 meV; between the two parameters the important one is the diffuse character (ζ) of the orbitals.

The third possibility we suggest to account for the large exchange coupling in **2** is based on the presence of large metal-metal interaction via *the nitrogen lone pairs separated by one C-C* σ bond. This idea was first put forward by Hoffmann.[20,25] To the best of our knowledge, this through-bond coupling has not been thoroughly investigated experimentally;[26] only weakly coupled species have been observed with a maximum value of -10.4 cm^{-1} for the singlet−triplet gap in a piperazine-bridged dimer. The original mechanism proposed by Hoffmann is summarized in the following. The essence of the through-bond mechanism is the interaction of the symmetric (n^+) and the antisymmetric (n^-) combinations of the nitrogen lone pairs with the C−C σ and σ^* orbitals (Figure 9). Thus the n^+ mixes with σ and as a result of the interaction is pushed to higher energy. On the other hand, n^- mixes with σ^* and is stabilized to lower energy as a consequence of that interaction. The n^+ and n^- combinations are, then, split with an energy gap δ which is at

(23) The molecule contains two asymmetric parts related by an inversion center; thus, the magnetic orbital is defined as the FMO containing the single electron in the asymetric unit.
(24) In the case of orthogonality between the equatorial and axial components ($\theta \approx 90°$), a ferromagnetic coupling is expected.
(25) Hoffmann, R. *Acc. Chem. Res.* **1971**, *4*, 1.
(26) (a) Chiari, B.; Hatfield, W. E.; Piovesana, O.; Tarantelli, T.; Ter Harr, L. W.; Zanazzi, P. F. *Inorg. Chem.* **1983**, *22*, 1468. (b) Chiari, B.; Piovesana, O.; Tarantelli, T.; Zanazzi, P. F. *Inorg. Chem.* **1984**, *23*, 2542.

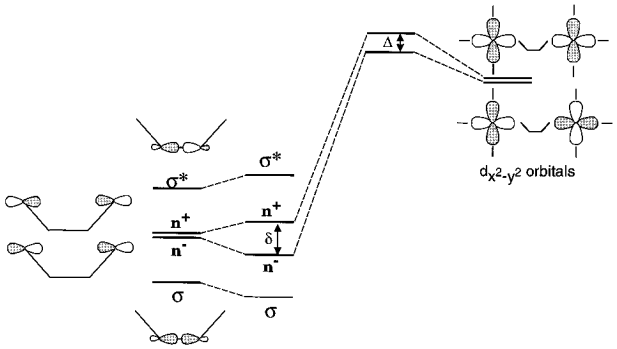

Figure 9. Hoffmann's orbital model of metal−metal interaction through three σ-bonds.

the origin of the Δ value between the magnetic orbitals in a dinuclear Cu(II) complex; these two magnetic orbitals would be otherwise degenerate.

The situation in **2** is more complex due to the presence of *two dissymmetric* N−C−C−N bridges. First, the presence of *two* bridges leads to four combinations[27a] of the nitrogen lone pairs, two of symmetry u and two of symmetry g as shown in Figure 10. Second, the *nonsymmetric nature* of the bridges with one tertiary amine nitrogen N(1) on one side and one amide nitrogen N(3) on the other allows the interaction of the four combinations *of the lone pairs* with the g and u bonding combination of the C−C σ orbitals[27b] the C−C σ* combinations being too high in energy to interact with the nitrogen lone pair combinations. When the interaction between the four combinations of the nitrogen lone pairs ($32a_g$, $33a_u$, $34a_u$ and $34a_g$) and the two C−C σ orbitals ($5a_g$, $5a_u$) of the fragment containing the two C(5)−C(6) bridges is take into account, six MO's of the ligands are obtained. The FMO analysis shows that only two among these six orbitals ($37a_g$ (−13.081 eV) and $40a_u$ (−12.518 eV)) are relevant for the interaction in the dinuclear complex. The $40a_u$ orbital stemming from the antibonding combination of the orbitals $33a_u$, $34a_u$, and $5a_u$ has a higher energy than the $37a_g$ orbital arising from the nonbonding combination of the $32a_g$, $34a_g$, and $5a_g$ orbitals (Figure 8). Finally, the large gap of 563 meV (δ_1) between the $37a_g$ and $40a_u$ orbitals is at the origin of the Δ value of 178 meV between the two $45a_g$ and $45a_u$ MO's of the dinuclear complex as shown in Figure 8.

(27) (a) g and u labels refer to the centrosymmetric nature of the dinuclear complex. (b) The g and u combinations of the σ C−C bonds are $N_1(\sigma_{c5-c6} + \sigma_{c5'-c6'})$ and $N_2(\sigma_{c5-c6} - \sigma_{c5'-c6'})$, respectively.

(28) Hall, D.; Waters, T. N. *J. Chem. Soc.* **1960**, 2644.
(29) (a) Svedung, D. H. *Acta Chem. Scand.* **1969**, *23*, 2865. (b) Watkins, N. T.; Dixon, E. E.; Crawford, V. H.; McGregor, K. T.; Hatfield, W. E. *J. Chem. Soc., Chem. Commun.* **1973**, 133.
(30) (a) Duckworth, V. F.; Stephenson, N. C. *Acta Crystallogr., Sect. B*, **1969**, *25*, 1795. (b) Bray, J. W. *Phys. Rev. Lett.* **1975**, *35*, 744.

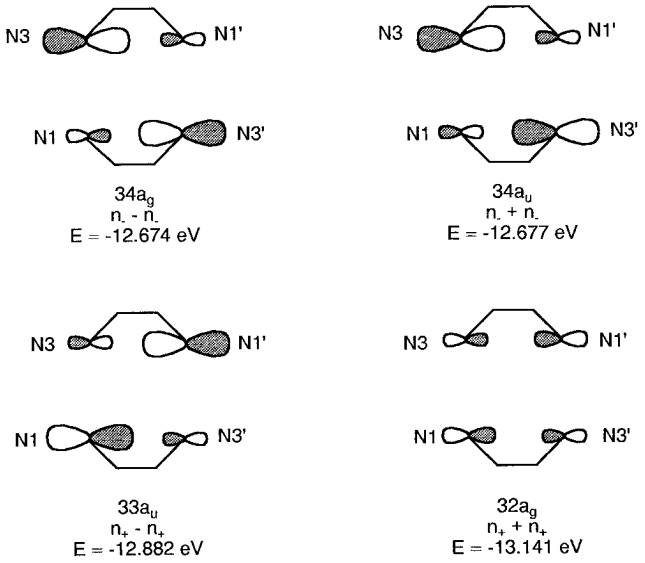

Figure 10. Schematic representation of the combinations of the lone pairs involved in the through-bond mechanism for **2**.

All these considerations show that it is the Hoffmann mechanism that accounts for the rather large observed *J* value in **2**.

Conclusion

The reaction between Cu(II) and a new macrobicyclic ligand affords a dinuclear complex. The structural studies show that the two Cu(II) ions are linked via two N−C−C−N sequences. A thourough analysis of the different possible exchange pathways within the dinuclear species using extended Hückel calculations showed that a through-bond mechanism involving the N−C−C−N sequences is operative. To the best of our knowledge, our complex is the first example where the Hoffmann mechanism accounts for a such large magnetic interaction between two Cu(II) ions. Furthermore, EPR studies show spectra typical of exciton triplets common in TCNQ derivatives but rare for coordination chemistry compounds.

Acknowledgment. This work was supported by the Programa de Acciones Integradas Hispano-Francesas and the DGICYT (Spain) through Project PB94-1002. We thank Doctor Geneviève Blondin for her technical assistance in the EPR study.

Supporting Information Available: Tables of atomic positional parameters for hydrogen atoms, anisotropic temperature factors for non-hydrogen atoms, and least-squares planes and a drawing of FMO's involved in the interaction mechanism for **2** (4 pages). Ordering information is given on any current masthead page.

IC950186G